Assessment of Series Resistance Components of a Solar PV Module Depending on its Temperature Under Real Operating Conditions

S. Bounouar*, R. Bendaoud*, H. Amiry*, B. Zohal*, F. Chanaa*, E. Baghaz*, C. Hajjaj**, S. Yadir***, A. El Rhassouli****, M. Benhmida*,‡.

*Laboratory of Electronics, Instrumentation and Energy (LEIE), Faculty of Science, Chouaib Doukkali University, Department of Physics, Route Ben Maachou,B.P 20, 24000 El Jadida, Morocco.

**Laboratory of Applied Sciences for the Environment and Sustainable Development, Higher School of Technology of Essaouira, Cadi Ayyad University, BP.383, Essaouira, Morocco.

***Laboratory of Materials, Processes, Environment and Quality, ENSA, Cadi Ayyad University, Safi, Morocco.

****Louis Aragon Technical High School, Academy of Franche Comté, Héricourt, France.

(bounouar.said@gmail.com, rbendaoud27@gmail.com, houssam.amiry@gmail.com, zohalbouchaib@gmail.com, fatimachanaa2020@gmail.com, e.baghaz@yahoo.fr, hajjaj.charaf@gmail.com,yadir1976@yahoo.fr, rhassouli@wanadoo.fr, benhmida@gmail.com)

‡ Corresponding Author; Postal address: Faculty of Science, Chouaib Doukkali University, Department of Physics, Route Ben Maachou, B.P 20,24000 El Jadida, Morocco; TEL: +212669828406; benhmida@gmail.com

Received: 08.08.2020 Accepted:16.09.2020

Abstract- Among the physical parameters of the standard single diode model of a solar cell, series resistance is one of those that strongly affects its performance. Contradictory changes in series resistance depending on temperature were reported in the literature. Accurate measurements of I-V characteristics were taken under different real operating conditions at constant temperature and solar irradiance, using a high-performance I-V curve tracer. The experimental results were used to determine series resistance of a photovoltaic module using two extraction methods. Empirical laws of series resistance components depending on module operating temperature were cheeked. It emerges that of the seven series resistance components, only four essentially determine its value.

Keywords Solar cell model, temperature effect, physical parameters, series resistance components, extraction method.

1. Introduction

The performances of a photovoltaic (PV) module are strongly depending on the environmental conditions such as the operating temperature and solar irradiance [1]–[3]. They are usually evaluated using the manufacturers datasheet provided under standard test conditions (STC) which are seldom encountered [2], [4]–[6]. Thus, it is recommended to perform accurate measurements, outdoor, under real operating conditions to determine the physical parameters related to the PV generator model and evaluate their variations [2], [4], [5].

Several models of a solar cell were proposed and represented by their equivalent electrical circuits using a number of physical parameters [7]–[12]. A number of extraction methods were developed to extract the values of these parameters [3], [13]–[18]. Series resistance (R_S) is a physical parameter assumed to be zero for an ideal solar cell and takes definite values for real solar cell [19]. It is related to the ohmic losses inside different regions of the solar cell [20]. When R_S increases, the ohmic losses increase and lead to a decrease in the electrical efficiency of the PV generators [19], [21], [22]. Therefore, it is very useful to carry out a detailed analysis of R_S evolution depending on temperature and evaluate its impact on PV generators performances. A number of studies have conducted to assess R_S using different extraction methods: graphical [23], numerical [24], and analytical methods [19], [23], [25], [26]. Some authors have found that R_S increases with increasing temperature [27]–[29] and others have reported the opposite for the same solar cell such as the crystalline technology [5], [30]–[32].

This paper presents a study of the evolution of R_S components characterizing a PV module depending on its operating temperature. A performing I-V curve tracer was used to take accurate measurements of I-V characteristics [2]. Some empirical laws were used to analyze the different components of R_S depending on temperature. The results are compared to those extracted by the method based on the combination of a genetic algorithm and the simulated annealing algorithm (CGSAA) [33], and those extracted by the iterative extraction method [8].

2. Materials and methods

2.1. Experimental setup

An appropriate experimental setup as shown in Fig.1, was used to investigate R_S behavior characterizing a PV module under its real operating conditions [2]. It includes an I-V curve tracer used to automatically varying load external resistances and scanning the entire I-V curve at a rate of one point ($I_{exp,i}$, $V_{exp,i}$) per msec [2]. The temperature was taken using a K Type thermocouple placed on the rear side of the PV module. Solar irradiance on the module plane was measured using SL-200 Solarimeter. The I-V curve tracer is controlled by an Arduino board [2]. The measurements were carried out on a monocrystalline PV module. Table 1 presents the manufacturer's datasheet.

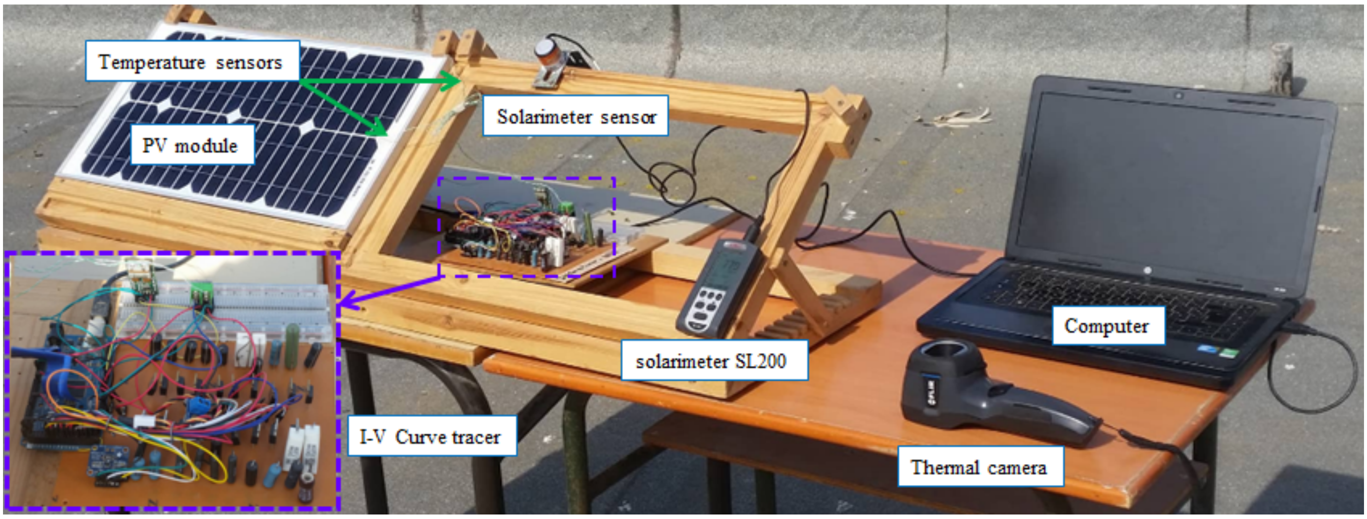

Fig. 1. Experimental setup.

Table 1. Manufacturer's datasheet of the PV module in STC.

PV module		TDC-M20-36
Technology		monocrystalline
Maximum power current (I_m)	[A]	1.07
Maximum power voltage (V_m)	[V]	18.76
Maximum power (P_{max})	[W]	20
Open circuit voltage (V_{OC})	[V]	22.7
Short circuit current (I_{SC})	[A]	1.17
Surface of the module (S)	[cm^2]	1569.96
Number of cells connected in series	(N_s)	36

2.2. Solar cell modeling

Fig.2 shows the electrical circuit of the standard single diode model of a PV cell [34]. This circuit is composed of a current generator (I_{ph}), a diode characterized by an ideality factor (n) and a reverse saturation current (I_0), a parallel resistance (R_{SH}) representing solar cell losses associated with the leakage currents through its junction and the peripheral surface, and a series resistance (R_S) taking into account the ohmic losses within the cell and metal semiconductor contacts. The study focuses on the influence of temperature on the evolution of R_S whose values are determined using two extraction methods.

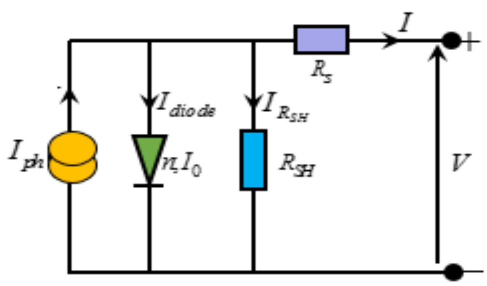

Fig. 2. Electrical circuit equivalent to the standard single diode model of a solar cell.

The current intensity (I) delivered by a solar cell and the output voltage (V) are linked by the following transcendent equation:

$$I = I_{ph} - I_0\left(exp\left(\frac{V+R_S I}{nV_{th}}\right) - 1\right) - \frac{V+R_S I}{R_{SH}} \tag{1}$$

Where $V_{th} = k_B T/q$ is the thermal voltage.

2.3. Computation of R_S components

Depending on their manufacturing technology, solar cell's efficiency decreases more or less significantly when their operating temperature increases. Based on equations describing power losses in different regions of a standard solar cell, Meier et al. [35], [36] have expressed the components of R_S according to their resistivities and the technological parameters related to the metal contact deposition processes (Tables 2 and 3). D. J. Crain et al. have showed [28] that R_S and n have more influence on solar cell efficiency than the other physical parameters in the model. M. A. da Luz et al [37] have expressed analytically the interdependence between R_S, R_{SH} and n. Fig. 3 shows that beyond certain values of n and R_{SH}, R_S no longer varies.

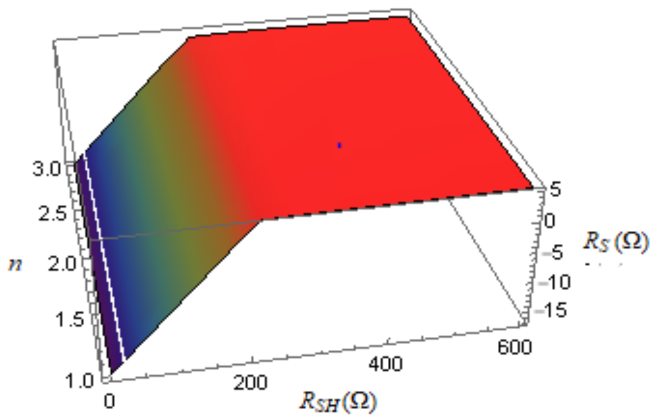

Fig. 3. Influence of n and R_{SH} on R_S.

The evaluation of the variations of each component depending on temperature can be made by the subdivision of a solar cell into unit cell elements. The front face contact is of a comb-shaped metal grid (Fig. 5 (a)) which can be cut into unit cell elements according to the shape shown in Fig. 5 (b). R_S is equivalent to the parallel association of the total unit cell elements.

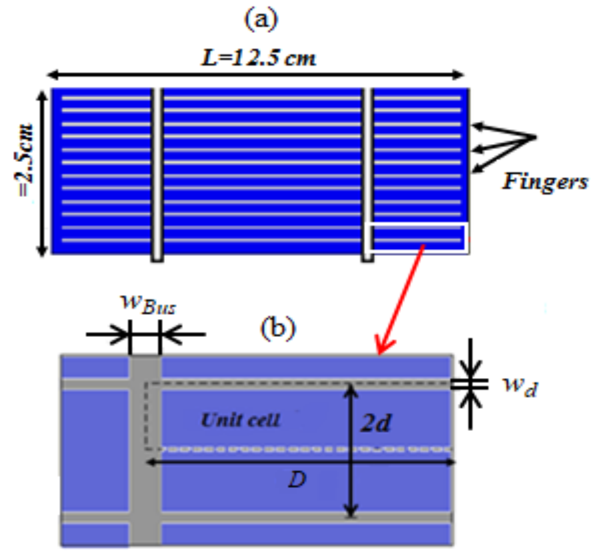

Fig. 5. (a) Solar cell sizes: cell width (l), and cell length (L). (b) Unit cell: width of the unit cell(d), busbar width(w_{Bus}), finger width (w_d), and unit cell length (D).

Meier et al. have decomposed R_S into seven components [35], [36] (Fig. 4): R_{Bus} (Busbars resistance), R_F (Fingers resistance), R_{FC} (Front contact resistance), R_E (Emitter resistance), R_B (Base resistance), R_{RC} (Rear contact resistance), and R_{RM} (The resistance of the rear metal sheet) [35], [36]. Hence:

$$R_S = R_{Bus} + R_F + R_{FC} + R_E + R_B + R_{RC} + R_{RM} \tag{2}$$

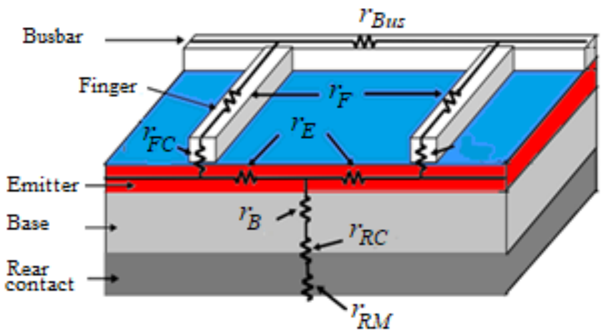

Fig. 4. R_S components of a common solar cell according to Meier et al. [35], [36].

Table 2. Technological parameters used for simulation and calculation of R_S with a comb-shaped metal grid on the front face [38].

Symbol	Description	Value	Unit
Fixed parameters common to screen-printed (sp) and electrochemical (ec) contacts			
e_B	Base layer thickness	2×10^{-2}	cm
w_{Bus}	Busbar width	0.2	cm
e_{RM}	Thickness of rear metal sheet	2×10^{-3}	cm
ρ_{RM}	Resistivity of the rear metal sheet	5.6×10^{-6}	Ω.cm
Fixed parameters of the screen-printed contacts			

$\rho_{Ag,sp}$	Resistivity of Ag metal on the cell front face	3.9×10^{-6}	Ω.cm
$\rho_{Ag,sp}$ [39]		7×10^{-6}	Ω.cm
$\rho_{Ag,sp}$ [35]		21.8×10^{-6}	Ω.cm
$2d_{sp}$	Space between two neighboring fingers	0.25	cm
$w_{d,sp}$	Finger width on the cell front face	1.2×10^{-2}	cm
$e_{d,sp}$	Finger thickness on the cell front face	1.5×10^{-3}	cm
$e_{Bus,sp}$	Busbar width on the cell front face	1.5×10^{-3}	cm
Fixed parameters of the electrochemical contacts			
$\rho_{Ag,ec}$	Resistivity of Ag metal on the front face	2.1×10^{-6}	Ω.cm
Variable parameters of the electrochemical contacts			
$2d_{ec}$	Space between two neighboring fingers	0 – 0.6	cm
$w_{d,ec}$	Finger width on the cell front face	10^{-3}- 10^{-2}	cm
$e_{d,ec}$	Finger thickness on the cell front face	10^{-4}- 2×10^{-3}	cm

Table 3. Components of R_S depending on temperature and technological parameters

R_S components	Mathematical form depending on temperature and technological parameters
Busbars resistance	$R_{Bus}=\frac{\rho_{f,0}(\mathrm{Ag})}{3}\frac{d^2}{w_{Bus}e_{Bus}}D.n_d{}^2\left(1+3.8\times10^{-3}\left(T-293\right)\right)$ [36] (3) With : $\rho_f(\mathrm{Ag})=\rho_{f,0}(\mathrm{Ag})\left[1+\alpha\left(T-T_0\right)\right]$ [40] (4)
Fingers resistance	$R_F=\frac{2\rho_{f,0}(\mathrm{Ag})}{3}\frac{d.D^2}{e_d.w_d}\left(1+3.8\times10^{-3}\left(T-293\right)\right)$ [36] (5)
Front contact resistance	$R_{FC}=d\sqrt{\rho_E\ \rho_{FC}(FE)/e_E}$ [38], [41] (6) Where: $\rho_{FC}(FE)=\left(\frac{q\pi A^*T}{k_B\sin\left(\pi C_1k_BT\right)}.\exp\left(\frac{-q\Phi_{Ag,n-Si}}{E_{00n}}\right)-\frac{qA^*}{C_1k_B^2}.\exp\left(\frac{-q\Phi_{Ag,n-Si}}{E_{00n}}-C_1E_{Fn}\right)\right)^{-1}$ [42], [43] (7) $\rho_E=\frac{6.24151\times10^{12}}{N_D}\left(\frac{7.4\times10^8}{\left(1+\frac{1.41535\times10^{-11}N_D}{T^{2.546}}\right)T^{2.33}}+\frac{0.227218}{T^{0.57}}\right)^{-1}$ [44] (8) $A^*=264221.719\sqrt{\frac{1}{1.17-\frac{7.02\times10^{-4}T^2}{1108+T}}}$ [45], [46] (9) $E_{Fn}=1.38066\times10^{-23}T\left(\frac{4.0699\times10^{-34}N_D{}^2}{T^{3.16}}+\frac{1.01377\times10^{-16}N_D}{T^{1.58}}+\ln\left(\frac{2.86738\times10^{-16}N_D}{T^{1.58}}\right)\right)$ [42] (10)

	$$E_{00n} = 3.6936\times10^{-30}\sqrt{N_D}\left(1.17-\frac{7.02\times10^{-4}T^2}{1108+T}\right)^{\frac{1}{4}} \text{ [42], [43]} \quad (11)$$ $$\Phi_{Ag,n-Si} = 0.6+\left(T-300\right)\left(\frac{7.02\times10^{-4}T^2}{\left(1108+T\right)^2}-\frac{1.404\times10^{-3}T}{1108+T}\right) \text{ [42]} \quad (12)$$ $$C_1 = \frac{1.35369\times10^{29}}{\sqrt{N_D}}\ln\left(\frac{6.40871\times10^{-19}\Phi_{Ag,n-Si}}{E_{Fn}}\right)\left(1.17-\frac{7.02\times10^{-4}T^2}{1108+T}\right)^{-\frac{1}{4}} \text{ [42], [43]} \quad (13)$$
Rear contact resistance	$$R_{RC} = \rho_{RC}(TFE) = \frac{k_B}{q.T.A^*}.C_{TFE}\exp\left(\frac{q\Phi_{Al,p-Si}}{E_0}\right) \text{ [42]} \quad (14)$$ Where : $$C_{TFE} = \frac{k_BT}{\sqrt{\pi\left(q\Phi_{Al,p-Si}+E_{Fp}\right)E_{00p}}}\cosh\left(\frac{E_{00p}}{k_BT}\right)\sqrt{\coth\left(\frac{E_{00p}}{k_BT}\right)}\exp\left(\frac{E_{Fp}}{E_0}-\frac{E_{Fp}}{k_BT}\right) \text{ [42]} \quad (15)$$ $$E_{Fp} = -1.38066\times10^{-23}T\ln\left(\frac{1.23399\times10^{-15}\ N_A}{T^{1.85}}\right) \text{ [42]} \quad (16)$$ $$E_{00p} = 3.6936\times10^{-30}\sqrt{N_A}\left(1.17-\frac{7.02\times10^{-4}T^2}{1108+T}\right)^{\frac{1}{4}} \text{ [42], [43]} \quad (17)$$ $$\Phi_{Al,p-Si} = 0.51+\left(T-300\right)\left(\frac{7.02\times10^{-4}T^2}{\left(1108+T\right)^2}-\frac{1.404\times10^{-3}T}{1108+T}\right) \text{ [42]} \quad (18)$$ $$E_0 = E_{00p}\coth\left(\frac{E_{00p}}{k_BT}\right) \text{ [47]} \quad (19)$$
Base resistance	$$R_B = \frac{6.24151\times10^{18}e_B}{N_A}\left(54.3\,T_n^{-0.57}+\frac{1.36\times10^8T^{-2.23}}{1+\left[N_A/\left(2.35\times10^{17}T_n^{2.4}\right)\right]^{0.88\,T_n^{-0.146}}}\right)^{-1} \text{ [36], [44]} \quad (20)$$
Emitter layer resistance	$$R_E = \frac{2.0805\times10^{18}d^2}{e_E\ N_D}\left(88\,T_n^{-0.57}+\frac{7.4\times10^8T^{-2.33}}{1+\left[N_D/\left(1.26\times10^{17}T_n^{2.4}\right)\right]^{0.88\,T_n^{-0.146}}}\right)^{-1} \text{ [36], [44]} \quad (21)$$
The resistance of the rear metal sheet	$$R_{RM} = \rho_{RM,0}(\mathrm{Al})\left(1\ +\ 3.9\times10^{-3}\left(T\ -\ 293\right)\right).e_{RM} \text{ [36]} \quad (22)$$
Resistance of the connection wires	$$R_t = 4.5\times10^{-6}\frac{l_t\,S}{h_tw_t}\left(1\ +\ 3.8\times10^{-3}\left(T\ -293\right)\right) \text{ [48]} \quad (23)$$

2.4. Methods for extracting physical parameters

- CGSAA method

CGSAA extraction method is based on a combination of a genetic algorithm and the simulated annealing algorithm [33]. The first algorithm consists of a subdivision of search domains of PV generator physical parameters into regular sub-domains whose the number, the upper, and the lower bounds were defined and discussed [33]. This procedure allows for determining the minimum of the root mean square error (*RMSE*) defined as follows [11], [49]:

$$RMSE(X)=\sqrt{\sum_{k=1}^{M}\left(f(V_{exp,k},I_{exp,k},X)\right)^2/M} \qquad (24)$$

Where M is the number of experimental ($I_{exp,k}$, $V_{exp,k}$) points of the characteristic and $f(V_{exp,k}, I_{exp,k}, X)$ represents the deviation between experimental and extracted current values, defined as follows [11], [49]:

$$f(V_{exp,k},I_{exp,k},X)=I_{exp,k}-\left\{I_{ph}-I_0\left(exp\left(\frac{V_{exp,k}+R_S I_{exp,k}}{nV_{th}}\right)-1\right)-\frac{V_{exp,k}+R_S I_{exp,k}}{R_{SH}}\right\} \qquad (25)$$

Where $X=(I_{ph}, I_0, n, R_S, R_{SH})$ is a solution vector of the physical parameter values.

The genetic algorithm starts with a random generation of a set of physical parameter values in each subdomain. The generated values are combined and evaluated using Eq. (24) to choose the best solution corresponding to the minimum of *RMSE(X)* in each subdomain. Then, the solutions obtained in different subdomains are crossed for refining the search. The assessment of obtained combinations after crossing allows choosing the best solution taken as an initial solution for the simulated annealing algorithm. This algorithm allows getting the optimal values of the researched physical parameters [33].

- Iterative method

The iterative method is based on the injection of test values of R_S or n in the characteristic equation (Eq. (1)) [8], [50], and generating several I-V characteristics built using the physical parameters (I_{ph}, R_S, n, R_{SH}, and I_0) taken in each iteration. Compatibility between each I-V characteristic generated and that obtained experimentally is checked using the error function *RMSE* (X) given by Eq. (24).

The error rate on R_S and n values is proportional to *RMSE*. The physical parameters (I_{ph}, R_S, n, R_{SH}, and I_0) selected after the extraction operation are those matching with the minimum value of *RMSE* [8].

3. Results and discussion

3.1. Experimental results

Fig. 6 shows the experimental I-V characteristics of the monocrystalline PV module for seven temperature values and constant solar irradiance, $G \approx 1000\ W/m^2$.

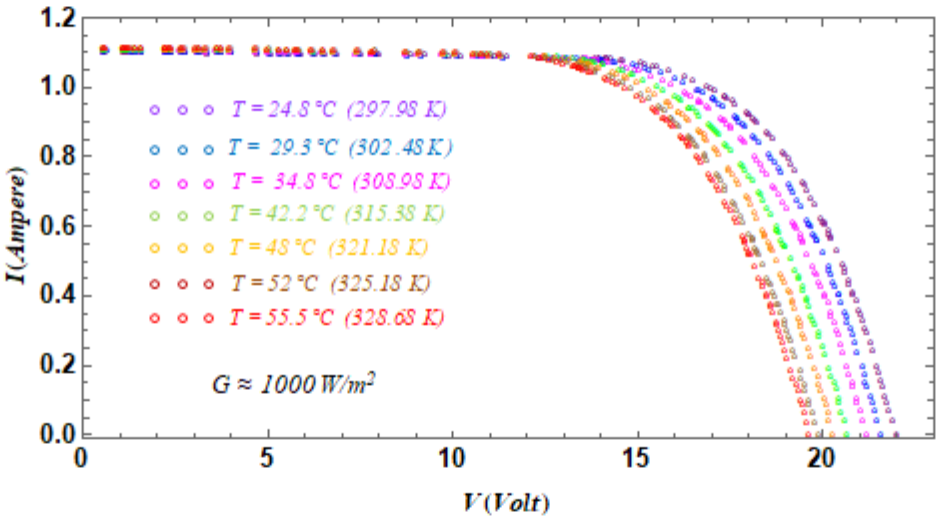

Fig. 6. Experimental I-V characteristics of the monocrystalline PV module for seven temperature values and constant solar irradiance, $G \approx 1000\ W/m^2$.

These characteristics were used to extract R_S values depending on temperature, using CGSAA and the iterative extraction methods. Table 4 shows the external physical parameters depending on temperature. When the module temperature increased from 297.98 K to 328.68 K, its maximum power increased from 16.92 to 14.45 W and the power losses due to R_S (P_{R_S}) increased from about 0.81 W to 0.95 as shown in Table 4.

Table 4. External physical parameters of the monocrystalline PV module measured outdoors for seven temperature values and constant solar irradiance, $G \approx 1000\ W/m^2$. P_{R_S} is the power losses due to R_S.

Temperature	[K]	297.98	302.48	308.98	315.38	321.18	325.18	328.68
I_m	[A]	0.9974	0.9944	0.9876	0.9921	0.9908	0.9915	0.9848
V_m	[V]	16.970	16.535	16.075	15.640	15.286	14.940	14.675
P_{max}	[W]	16.92	16.44	15.88	15.52	15.15	14.81	14.45
V_{OC}	[V]	22.043	21.628	21.250	20.730	20.340	19.940	19.800
I_{SC}	[A]	1.0999	1.1023	1.1036	1.1093	1.1097	1.1115	1.1132
P_{R_S}	[W]	0.8094	0.8259	0.8427	0.8787	0.9365	0.9732	0.9496

3.2. Assessment of R_S components depending on temperature

The influence of the operating temperature of the PV module on R_S components was evaluated using Eq. (2) to Eq. (22) (Fig. 7). Simulations were carried out taking into account the technological parameters related to the two methods of depositing metal contacts as mentioned above (Tables 2 and 3) [38].

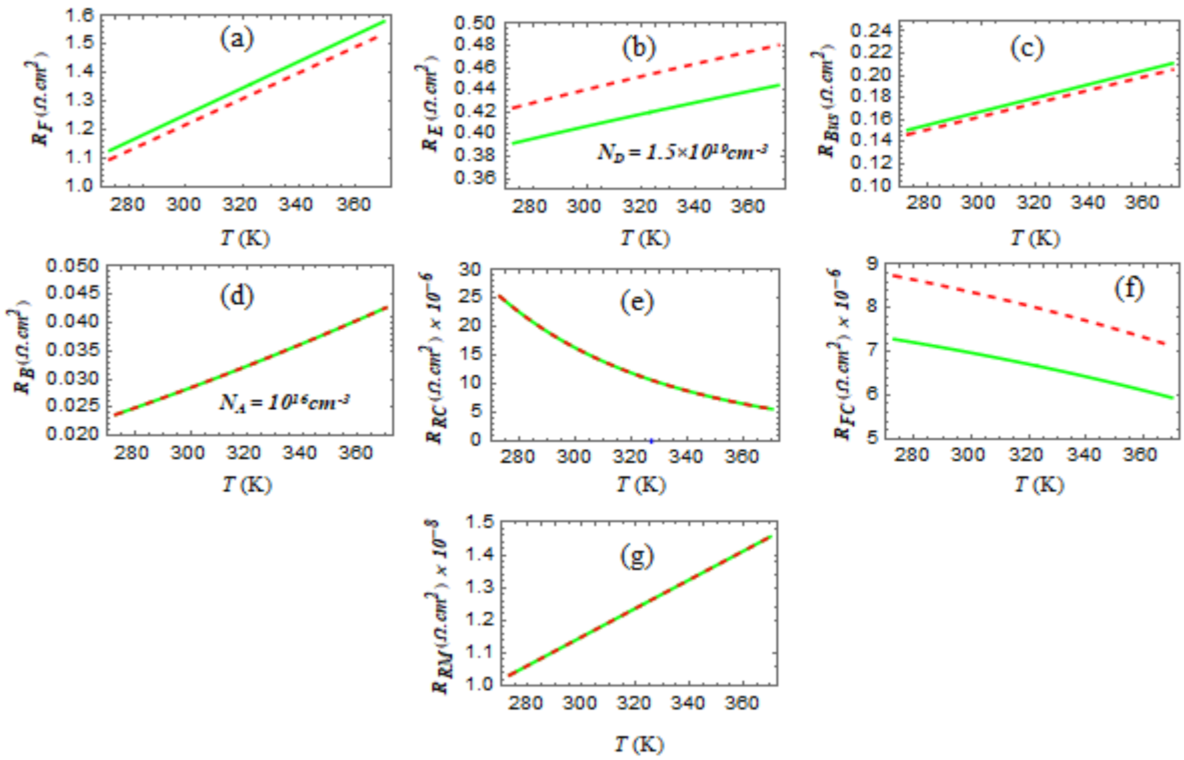

Fig. 7. Evolution of R_F(a), R_{Bus}(b), R_B(c), R_E(d), R_{RC}(e), R_{FC}(f), R_{RM}(g) depending on temperature taking into account the technological parameters associated with the method of depositing metal contacts by the screen- printing (—) and by the electrochemistry (---).

Fig. 7 (a-d) show the predominant components of R_S. They are in descending order of weight: R_F (fingers resistance), R_{Bus} (busbars resistance), R_B (base resistance), and R_E (emitter resistance). These results are in good agreement with those reported in the literature [35], [36]. The front contact and rear contact resistances (R_{FC} and R_{RC}) become negligible to the highest temperatures (Fig. 7 (e, f)), as was reported by Kwang-Hoon Oh et al. and H. N. Tran et al. [42], [51]. R_{RM} is also negligible due to the small thickness of the metal layer (Fig. 7 (g)). Except R_{FC} and R_{RC}, all other R_S components increase when the temperature increases. R_F, R_{Bus}, and R_{RM} increase linearly with temperature in contrast to R_E and R_B. Hence, the increase in R_S with the temperature is mainly due to the metal grid resistance (fingers, busbars), base resistance, and the emitter resistance.

3.3. Evolution of extracted physical parameters depending on temperature

Table 5 shows that with the exception of R_{SH}, the other physical parameters assessed using the two extraction methods (CGSAA and iterative method) are well compatible for all measured operating temperatures of the PV module.

Table 5. Physical parameters extracted by CGSAA and the iterative methods for seven temperature values of the monocrystalline module.

	T (K)	297.98	302.48	308.98	315.38	321.18	325.18	328.8
Physical parameters extracted by CGSAA method	**R_S (Ω)**	**0.0226**	**0.0232**	**0.0240**	**0.0248**	**0.0265**	**0.0275**	**0.0272**
	R_{SH} (Ω)	226.29	182.87	171.35	158.79	136.15	114.47	94.54
	I_0 (µA)	4.0884	5.5606	7.9560	11.1596	12.2895	15.3169	17.2342
	n	1.9057	1.8896	1.8781	1.8426	1.7910	1.7669	1.7476
	I_{ph} (A)	1.0985	1.0989	1.1028	1.1070	1.1078	1.1080	1.1146
RMSE		0.004285	0.004192	0.004133	0.003949	0.004114	0.003603	0.004177
Physical parameters extracted by iterative method	**R_S (Ω)**	**0.023**	**0.024**	**0.024**	**0.026**	**0.026**	**0.026**	**0.026**
	R_{SH} (Ω)	2257.24	83.88	211.40	537. 62	240.63	1176.43	706.49
	I_0 (µA)	3.9414	4.5657	8.0505	9.6657	13.0558	19.1338	21.8385
	n	1.90	1.86	1.88	1.82	1.80	1.80	1.79
	I_{ph} (A)	1.0974	1.0995	1.1021	1.1057	1.1073	1.1090	1.1096
RMSE		0.004243	0.004177	0.004129	0.003855	0.004076	0.003843	0.004102

Table 5 shows that for the temperature range from 298 to 329 K and $G \approx 1000\ W/m^2$, the values of extracted n using CGSAA and the iterative methods decrease by about 0.0051 /K and 0.0036 /K, respectively. This reduction was attributed by Cotfas et al. [52] to temperature effects on the surface and Shockley-Read-Hall recombination mechanisms, the decrease in the resistance of the semiconductor active layer, and the trapping-detrapping phenomenon.

The extracted values of I_0 through CGSAA and the iterative methods increase by 0.43 µA/K and 0.58 µA/K, respectively. This is likely due, at least in part, to additional thermal activation of the charge carriers, as reported by Fébba et al. and Ghani et al. [5], [27]. The I_{ph} values extracted by the CGSAA method and the iterative method are also of the same order of magnitude and grow by 0.52 mA/K and 0.40 mA/K, respectively.

Otherwise, the extracted values of R_{SH} using the CGSAA method decrease by about 4.29 Ω/K. The reduction of R_{SH} was attributed by Cuce et al. [30] to the combined effects of trapping-detrapping and tunneling of charge carriers by localized defect levels in the material bandgap. On the other hand, the extracted values of R_{SH} by the iterative method show significant fluctuations. It should be noted that any arbitrary change, however small, in the value of n or R_S results in a relatively significant change in the value of R_{SH}. This indicates that R_{SH} has less influence on the optimization process with this method than the rest of the physical parameters.

Fig. 8 illustrates the changing of the extracted R_S values as a function of temperature using the two extraction methods previously described. The values of R_S calculated using the empirical laws specific to each of its components (Eq. (2) to Eq. (23)) make it possible to verify the reliability of these laws in the studied temperature range from 298 K to 329 K.

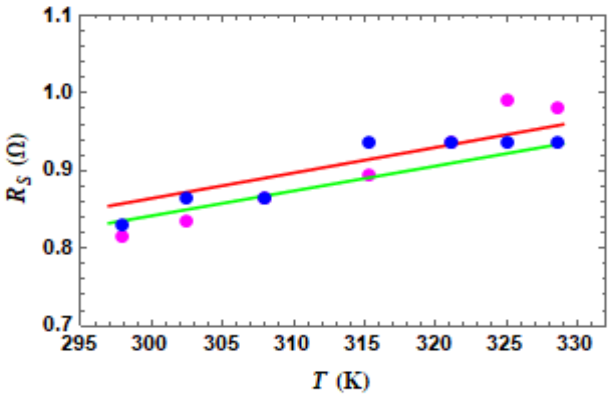

Fig. 8. Change in R_S as a function of temperature of the monocrystalline PV module obtained using the empirical laws for depositing metal contacts by screen printing (—) and by electrochemistry (—) methods. Values of R_S extracted using the iterative extraction method (●), and the CGSAA method (●).

Extracted R_S values using CGSAA and the iterative methods increase by 0.0035 Ω/K, and 0.0053 Ω/K, respectively, for the operating temperature of the PV module from 298 K to 329 K (Fig. 8). Using empirical laws (Eq. (2) to Eq. (23)), the resulting R_S increases by 0.0032 Ω/K for both methods of depositing metal contacts. A similar evolution of R_S was also reported by Bensalem et al. and Ding et al. [53], [54].

Fig. 8 shows that the values extracted by the iterative and CGSAA methods and those obtained using empirical laws are quite similar.

4. Conclusion

Resistive losses have a significant impact on the photovoltaic solar cells performances. The power dissipated by R_S represents approximately 6% of the power supplied by the PV module. Based on a detailed analysis of the R_S components, it is clear that the increase in R_S with temperature is governed by the increasing of four components. For the two methods of metal contacts deposition, the fingers resistance represents a significant part of more than 75%, followed by the busbars resistance the base resistance and the emitter resistance with about 12 %, 7%, and 3%, respectively. It would be interesting to operate over wider temperature ranges in order to check the reliability of some empirical laws describing the variations of R_S as a function of PV generators operating temperature.

Nomenclature

PV Photovoltaic
sp screen printing
ec electrochemistry
SDM Single Diode Model
IR Infrared
FE Field Emission
TFE Thermionic Field Emission
STC Standard test conditions (T = 25 °C, G_0= 1000 W/m^2 and AM = 1.5)
I Module terminal Current [A]
V Module output voltage [V]
I_{exp} Experimental module terminal Current [A]
V_{exp} Experimental module output voltage [V]
N_S Cells number connected in series
G Solar irradiation on a model plane [W/m^2]
R_S Series resistance [Ω]
R_{SH} Shunt resistance [Ω]
I_{ph} Photo-generated current [A]
I_{SC} Short circuit current [A]
I_0 Reverse saturation current [A]
I_m Maximum power current [A]
V_{OC} Open circuit voltage [V]
I_{exp} Experimental module terminal Current [A]
V_{exp} Experimental module output voltage [V]
V_m Maximum power voltage [V]
n Ideality factor
V_{th} Thermal voltage [V]
P_{max} Maximum power [W]
L Length of solar cell [cm]
l Width of solar cell [cm]

(Eq. 12)
R_{Bus} Busbars resistance of [Ω. cm^2]
e_{Bus} Thickness of busbar [cm]
d Width of the unit cell [cm]
w_{Bus} Width of a busbar [cm]
D Length of unit cell [cm]
T Module operating temperature [°C/K]
n_d Number of fingers

(Eq. 13)
α Thermal resistance coefficient
$\rho_{f,0}$(Ag) Silver resistivity at room temperature [Ω. cm]

(Eq. 14)
R_F Fingers resistance [Ω. cm^2]
w_d Width of a finger [cm]
e_d Thickness of each finger [cm]

(Eq. 15)
R_{FC} Front contact resistance [Ω. cm^2]
e_E Thickness of emitter sheet [cm]
ρ_E Emitter sheet resistivity [Ω. cm]
ρ_{FC}(FE)Front contact resistivity related to FE [Ω.cm]

(Eq. 16)
A* Richardson constant
k_B Boltzmann constant [=1.3806×10^{-23} J/K]
C_1 Parameter related to FE
E_{00n} Characteristic energy for Ag/N-Si interface [eV]
q Electron charge [=1.602×10^{-19} C]
$\Phi_{Ag,n\text{-}Si}$ Barrier height of Ag/N-Si contact [eV]

E_{Fn} Fermi energy with respect to the energy band edge in N-doped silicon [eV]

(Eq. 17)

N_D Doping concentration of emitter [1/cm^3]

(Eq. 23)

R_{RC} Rear contact resistance [Ω. cm^2]

ρ_{RC} Rear contact resistivity [Ω. cm]

C_{TFE} Parameter related to *TFE*

$\Phi_{Al,p\text{-}Si}$ Barrier height of Al/P-Si contact [eV]

E_0 Measure of the tunneling effect probability specific to *TFE* [eV]

(Eq. 24)

E_{Fp} Fermi energy with respect to the energy band edge in N-doped silicon [eV]

E_{00p} Characteristic energy for Al/P-Si interface [eV]

(Eq. 25)

N_A Doping concentration of base [1/cm^3]

(Eq. 29)

R_B Base resistance [Ω. cm^2]

e_B Thickness of base [cm]

T_n Normalized temperature [K]

(Eq. 30)

R_E Emitter resistance [Ω. cm^2]

(Eq. 31)

R_{RM} The resistance of the rear metal sheet [Ω. cm^2]

e_{RM} Thickness of the rear metal sheet [cm]

$\rho_{RM,0}$ Resistivity of the rear metal sheet at the reference temperature [Ω. cm].

(Eq. 32)

R_t Connection wires resistance [Ω. cm^2]

h_t Thickness of connection wire [cm]

w_t Width of connection wire [cm]

l_t Length of connection wire [cm]

S Solar cell surface [cm^2]

References

[1] B. Hüttl, L. Gottschalk, S. Schneider, D. Pflaum, and A. Schulze, " Accurate performance rating of photovoltaic modules under outdoor test conditions ", Solar Energy, vol. 177, p. 737-745, janv. 2019.

[2] H. Amiry, M. Benhmida, R. Bendaoud, C. Hajjaj, S. Bounouar, S. Yadir, K. Raïs, and M. Sidki, " Design and implementation of a photovoltaic I-V curve tracer: Solar modules characterization under real operating conditions ", Energy Conversion and Management, vol. 169, p. 206-216, août 2018.

[3] Y. Chaibi, A. Allouhi, M. Malvoni, M. Salhi, and R. Saadani, " Solar irradiance and temperature influence on the photovoltaic cell equivalent-circuit models ", Solar Energy, vol. 188, p. 1102-1110, août 2019.

[4] C. S. Ruschel, F. P. Gasparin, E. R. Costa, and A. Krenzinger, "Assessment of PV modules shunt resistance dependence on solar irradiance ", Solar Energy, vol. 133, p. 35-43, août 2016.

[5] D. M. Fébba, R. M. Rubinger, A. F. Oliveira, and E. C. Bortoni, "Impacts of temperature and irradiance on polycrystalline silicon solar cells parameters ", Solar Energy, vol. 174, p. 628-639, nov. 2018.

[6] S. Gaiotto, A. Laudani, F. R. Fulginei, and A. Salvini, " An advanced measurement equipment for the tracing of photovoltaic panel I–V curves ", 4th International conference on renewable energy research and applications, Palermo, Italy, nov. 2015, p. 1010-1014.

[7] M. R. AlRashidi, M. F. AlHajri, K. M. El-Naggar, and A. K. Al-Othman, " A new estimation approach for determining the I–V characteristics of solar cells ", Solar Energy, vol. 85, no 7, p. 1543-1550, juill. 2011.

[8] S. Yadir, S. Assal, A. El Rhassouli, M. Sidki, and M. Benhmida, " A new technique for extracting physical parameters of a solar cell model from the double exponential model (DECM) ", Optical Materials, vol. 36, no 1, p. 18-21, nov. 2013.

[9] A. N. Celik, " Artificial neural network modelling and experimental verification of the operating current of mono-crystalline photovoltaic modules ", Solar Energy, vol. 85, no 10, p. 2507-2517, oct. 2011.

[10] E. Q. B. Macabebe, C. J. Sheppard, et E. E. van Dyk, " Parameter extraction from I–V characteristics of PV devices ", Solar Energy, vol. 85, no 1, p. 12-18, janv. 2011.

[11] X. Gao, Y. Cui, J. Hu, G. Xu, Z. Wang, J. Qu, and H. Wang, " Parameter extraction of solar cell models using improved shuffled complex evolution algorithm ", Energy Conversion and Management, vol. 157, p. 460-479, févr. 2018.

[12] M. T. Ahmed, T. Goncalves, and M. Tlemcani, " Single diode model parameters analysis of photovoltaic cell ", 5th International conference on renewable energy research and applications, Birmingham, nov. 2016, p. 396-400.

[13] R. Abbassi, A. Abbassi, M. Jemli, and S. Chebbi, " Identification of unknown parameters of solar cell models: A comprehensive overview of available approaches ", Renewable and Sustainable Energy Reviews, vol. 90, p. 453-474, juill. 2018.

[14] D. Allam, D. A. Yousri, and M. B. Eteiba, " Parameters extraction of the three-diode model for the multi-crystalline solar cell/module using Moth-Flame Optimization Algorithm ", Energy Conversion and Management, vol. 123, p. 535-548, sept. 2016.

[15] S. Yadir, H. Amiry, R. Bendaoud, A. El Hassnaoui, A. Obbadi, M. Benhmida, and M. El Aydi, "Physical parameters extraction by a new method using solar cell models with various ideality factors ", in 2015 27th International Conference on Microelectronics (ICM), Casablanca, déc. 2015, p. 323-326.

[16] F. Ghani, G. Rosengarten, and M. Duke, " The characterisation of crystalline silicon photovoltaic devices using the manufacturer supplied data ", Solar Energy, vol. 132, p. 15-24, juill. 2016.

[17] F. Masmoudi, F. Ben Salem, and N. Derbel, " Identification of Internal Parameters of a Mono-Crystalline Photovoltaic Cell Models and Experimental Ascertainment ", International Journal of Renewable Energy Research, vol. 4, no 4, p. 840-848, 2014.

[18] J. Cubas, S. Pindado, and A. Farrahi, " New method for analytical photovoltaic parameter extraction ", International conference on renewable energy research and applications, Madrid, oct. 2013, p. 873-877.

[19] R. Singh, M. Sharma, R. Rawat, and C. Banerjee, " An assessment of series resistance estimation techniques for different silicon based SPV modules ", Renewable and Sustainable Energy Reviews, vol. 98, p. 199-216, déc. 2018.

[20] F. Frühauf, Y. Sayad, and O. Breitenstein, " Description of the local series resistance of real solar cells by separate horizontal and vertical components ", Solar Energy Materials and Solar Cells, vol. 154, p. 23-34, sept. 2016.

[21] B. Bora, O.S. Sastrya, R. Singha, M. Bangara, S. Raia , Renua, Y. Singha, R. Singha, B. K. Dasb, F. Azlanb , P. Anandb, R. Kuberb, and V. Krishnanb, " Series Resistance Measurement of Solar PV Modules Using Mesh in Real Outdoor Condition ", Energy Procedia, vol. 90, p. 503-508, déc. 2016.

[22] S. C. Swain, R. Dash, S. M. Ali, and A. K. Mohanta, "Performance evaluation of photovoltaic system based on solar cell modelling ", International Conference on Circuit, Power and Computing Technologies, mars 2015, p. 1-6.

[23] D. Pysch, A. Mette, and S. W. Glunz, " A review and comparison of different methods to determine the series resistance of solar cells ", Solar Energy Materials and Solar Cells, vol. 91, no 18, p. 1698-1706, nov. 2007.

[24] L. E. Peñaranda Chenche, O. S. Hernandez Mendoza, and E. P. Bandarra Filho, " Comparison of four methods for parameter estimation of mono- and multi-junction photovoltaic devices using experimental data ", Renewable and Sustainable Energy Reviews, vol. 81, p. 2823-2838, janv. 2018.

[25] Y. S. Kim, S.-M. Kang, B. Johnston, and R. Winston, "A novel method to extract the series resistances of individual cells in a photovoltaic module ", Solar Energy Materials and Solar Cells, vol. 115, p. 21-28, août 2013.

[26] N. Tutkun, E. Elibol, and M. Aktas, "Parameter extraction from a typical PV module using a metaheuristic technique ", 4th International conference on renewable energy research and applications, Palermo, Italy, nov. 2015, p. 755-759.

[27] F. Ghani, G. Rosengarten, M. Duke, and J. K. Carson, " On the influence of temperature on crystalline silicon solar cell characterisation parameters ", Solar Energy, vol. 112, p. 437-445, févr. 2015.

[28] D. J. Crain, S. E. Rock, J. E. Garland, and D. Roy, "Comparison of D.C. and A.C. electro-analytical methods for measuring diode ideality factors and series resistances of silicon solar cells ", Current Applied Physics, vol. 13, no 9, p. 2087-2097, nov. 2013.

[29] A. Ben Or and J. Appelbaum, " Dependence of multi-junction solar cells parameters on concentration and temperature ", Solar Energy Materials and Solar Cells, vol. 130, p. 234-240, nov. 2014.

[30] E. Cuce, P. M. Cuce, and T. Bali, " An experimental analysis of illumination intensity and temperature dependency of photovoltaic cell parameters ", Applied Energy, vol. 111, p. 374-382, nov. 2013.

[31] Y. Izumi and Y. Ueda, " Calculation of Degradation Rates of Poly Crystalline Si and CIGS PV Module using Outdoor Linear Interpolation Method ", 7th International conference on renewable energy research and applications, Paris, France, oct. 2018, p. 365-370.

[32] K. Tsuboi, T. Matsuoka, and T. Yachi, " An output degradation of photovoltaic module by fine particles deposition ", 2th International conference on renewable energy research and applications, nov. 2012, p. 1-5.

[33] R. Bendaoud, H. Amiry, M. Benhmida, B. Zohal, S. Yadir, S. Bounouar, C. Hajjaj, E. Baghaz, and M. El Aydi, " New method for extracting physical parameters of PV generators combining an implemented genetic algorithm and the simulated annealing algorithm ", Solar Energy, vol. 194, p. 239-247, déc. 2019.

[34] M. B. Prince, " Silicon Solar Energy Converters ", Journal of Applied Physics, vol. 26, no 5, p. 534-540, mai 1955.

[35] D. L. Meier, E. A. Good, R. A. Garcia. B. L. Bingham, S. Yamanaka, V. Chandrasekaran, and C. Bucher., " Determining Components of Series Resistance from Measurements on a Finished Cell ", 2006, p. 1315-1318.

[36] D. L. Meier and D. K. Schroder, "Contact resistance: Its measurement and relative importance to power loss in a solar cell ", IEEE Transactions on Electron Devices, vol. 31, no 5, p. 647-653, mai 1984.

[37] C. M. A. da Luz, F. L. Tofoli, P. dos Santos Vicente, and E. M. Vicente, " Assessment of the ideality factor on the performance of photovoltaic modules ", Energy Conversion and Management, vol. 167, p. 63-69, juill. 2018.

[38] C. Boulord, "Développement de techniques de métallisation innovantes pour cellules photovoltaïques à haut rendement ", Thèse de doctorat, L'Institut National des Sciences Appliquées, Lyon, 2012.

[39] P. N. Vinod, B. C. Chakravarty, M. Lal, R. Kumar, and S. N. Singh, "A novel method for the determination of the front contact resistance in large area screen printed silicon solar cells ", Semiconductor Science and Technology, vol. 15, no 3, p. 286-290, mars 2000.

[40] P. Hofmann, Solid State Physics: An Introduction. John Wiley & Sons, 2015.

[41] A. Goetzberger, J. Knobloch, and B. Voss, Crystalline silicon solar cells. Chichester : New York: Wiley, 1998.

[42] O. Kwang-Hoon, C. Jung-Hoon, K. Banerjee, C. Duvvury, and R. W. Dutton, " Modeling of temperature dependent contact resistance for analysis of ESD reliability ", 2003, p. 249-255.

[43] A. Y. C. Yu, " Electron tunneling and contact resistance of metal-silicon contact barriers ", Solid-State Electronics, vol. Vol. 13, p. 239-247, 1970.

[44] N. D. Arora, J. R. Hauser, and D. J. Roulston, " Electron and hole mobilities in silicon as a function of concentration and temperature ", IEEE Transactions on Electron Devices, vol. 29, no 2, p. 292-295, févr. 1982.

[45] F. A. Padovani, " The Richardson constant for thermionic emission in Schottky barrier diodes ", Solid-State Electronics, vol. 12, no 2, p. 135–136, 1969.

[46] C. R. Crowell, " Richardson constant and tunneling effective mass for thermionic and thermionic-field emission in Schottky barrier diodes ", Solid-State Electronics, vol. 12, no 1, p. 55-59, janv. 1969.

[47] K. Varahramyan and E. J. Verret, " A model for specific contact resistance applicable for titanium silicide-silicon contacts ", Solid-State Electronics, vol. 39, no 11, p. 1601-1607, nov. 1996.

[48] A. Mette, " New Concepts for Front side metalisation ", Thèse de doctorat, Universität Freiburg im Breisgau, 2007.

[49] J. P. Ram, T. S. Babu, T. Dragicevic, and N. Rajasekar, " A new hybrid bee pollinator flower pollination algorithm for solar PV parameter estimation ", Energy Conversion and Management, vol. 135, p. 463-476, mars 2017.

[50] D. S. H. Chan, J. R. Phillips, and J. C. H. Phang, " A comparative study of extraction methods for solar cell model parameters ", Solid-State Electronics, vol. 29, no 3, p. 329-337, mars 1986.

[51] H. N. Tran, T. A. Bui, A. M. Collins, and A. S. Holland, " Consideration of the Effect of Barrier Height on the Variation of Specific Contact Resistance With Temperature ", IEEE Trans. Electron Devices, vol. 64, no 1, p. 325-328, janv. 2017.

[52] D. T. Cotfas, P. A. Cotfas, and O. M. Machidon, " Study of Temperature Coefficients for Parameters of Photovoltaic Cells ", International Journal of Photoenergy, vol. 2018, p. 1-12, 2018.

[53] S. Bensalem and M. Chegaar, " Thermal behavior of parasitic resistances ", Revue des Energies Renouvelables, vol. Vol. 16, no N°1, p. 171-176, 2013.

[54] J. Ding, X. Cheng, and T. Fu, " Analysis of series resistance and P–T characteristics of the solar cell", Vacuum, vol. 77, no 2, p. 163-167, janv. 2005.